Biophysical Journal, Volume *112*

Supplemental Information

Hydrodynamic Hunters

Hossein Jashnsaz, Mohammed Al Juboori, Corey Weistuch, Nicholas Miller, Tyler Nguyen, Viktoria Meyerhoff, Bryan McCoy, Stephanie Perkins, Ross Wallgren, Bruce D. Ray, Konstantinos Tsekouras, Gregory G. Anderson, and Steve Pressé

Supporting Material

Hydrodynamic Hunters

Hossein Jashnsaz, Mohammed Al Juboori, Corey Weistuch, Nicholas Miller†, Tyler Nguyen†, Viktoria Meyerhoff‡, Bryan McCoy‡, Stephanie Perkins‡, Ross Wallgren‡, Bruce D. Ray, Konstantinos Tsekouras, Gregory G. Anderson *, Steve Pressé *

∗ **Corresponding authors. Email: stevenpresse@gmail.com (S.P.); ga2@iupui.edu (G.G.A)**

† These authors contributed equally to this work.

‡ These authors contributed equally to this work.

Supporting Material Methods

I. Algorithm to calculate the "signed curvature" (helicity)

We consider three adjacent points on a trajectory (i^{th} trajectory) in a 2D Cartesian coordinate system as $\mathbf{r_{j-1}}(x_{j-1}, y_{j-1})$, $\mathbf{r_j}(x_j, y_j)$, and $\mathbf{r_{j+1}}(x_{j+1}, y_{j+1})$ (Fig. S1A). Throughout this calculation, we use i as the trajectory index, and j as the point (frame) index on a specific trajectory. At the middle point, the absolute value of the curvature, designated by $\varkappa_j$, is

$$\varkappa_j = \frac{|c_j|}{[1 + (dy/dx|_j)^2]^{3/2}}. \tag{1}$$

where

$$c_j = \frac{d^2y}{dx^2}|_j = \frac{m_{1j} - m_{2j}}{(x_{j+1} - x_{j-1})/2}, \tag{2}$$

$$m_{1j} = \frac{y_j - y_{j-1}}{(x_j - x_{j-1})}, \tag{3}$$

$$m_{2j} = \frac{y_{j+1} - y_j}{(x_{j+1} - x_j)}, \tag{4}$$

$$\frac{dy}{dx}|_j = \frac{m_{1j} + m_{2j}}{2}. \tag{5}$$

We define the sign, φ_j, for the curvature as follows

$$\varphi_j = \frac{y_j - y_M}{|y_j - y_M|} \frac{x_{j+1} - x_{j-1}}{|x_{j+1} - x_{j-1}|} = \begin{cases} +1 & \text{for } cw, \\ -1 & \text{for } ccw, \end{cases} \tag{6}$$

where cw is for clockwise and ccw is for counterclockwise and where

$$y_M = y_{j-1} + (x_{j+1} - x_j) \frac{y_{j+1} - y_{j-1}}{(x_{j+1} - x_{j-1})}. \tag{7}$$

Now we define the signed curvature or helicity as:

$$\kappa_j = \varphi_j \varkappa_j. \tag{8}$$

We repeat the same calculation for all points (excluding the first and the last point) along the i^{th} trajectory then find the average curvature for this trajectory using $\bar{\kappa_i} = \frac{1}{M_i - 2} \sum_{j=2}^{M_i - 1} \kappa_j$, where M_i is the number of points (frames) along the i^{th} trajectory. We define the effective radius for the i^{th} trajectory as $R_i = 1/\bar{\kappa_i}$. Then we find the mean curvature and mean effective radius of N such trajectories ($\bar{\kappa} = \frac{1}{N} \sum_{i=1}^{N} \kappa_i$, $\bar{R} = \frac{1}{N} \sum_{i=1}^{N} R_i$). Negative values of R_i or $\bar{R}$ represent a ccw rotational direction. As an example, we apply this algorithm on synthetic ccw and cw circular trajectories in Fig. S1.

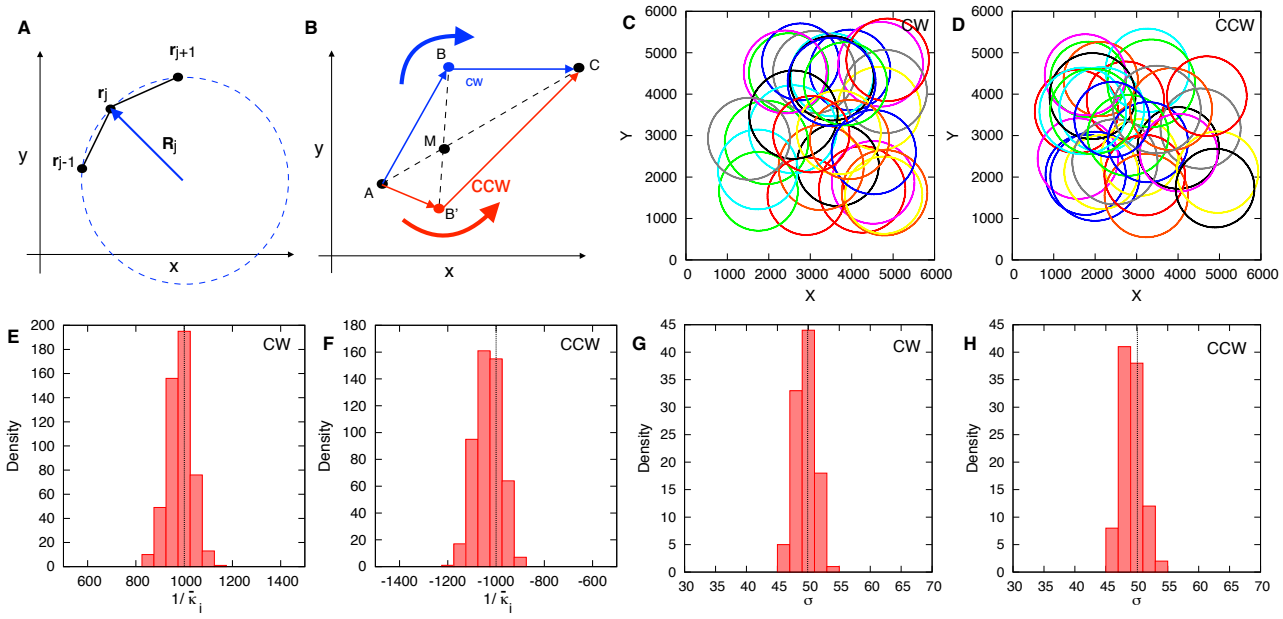

FIGURE S1. Illustration of our algorithm for computing signed curvatures (helicities). (A) We calculate the curvature by having 3 data points (curvature around midpoint) using Eq. 1 in Supplementary Text, and the radius of a circle – going through all 3 points – is approximated by this curvature in the limit that step sizes are much smaller than the radius. (B) We quantitively define a "signed curvature" (helicity) as follows: We consider the following data points: $A(x_{j-1}, y_{j-1}), C(x_{j+1}, y_{j+1}), M(x_M, y_M)$, $B(x_j, y_j)$, and $B'(x_j, y_j)$. ABC represents a cw helicity while $AB'C$ represents a ccw helicity. In this specific case, if $y_j > y_M$ the curve is cw, for $y_j < y_M$ the curve is ccw, and for $y_j = y_M$ it would be a straight line. M is the intersection of a line parallel to the y-axis from B (or equivalently from B' for ccw curve) and AC. This is how we use Eq. 6 and Eq. 7 in Supplementary Text, to define the sign of the curvature for the most general case. In order to test this algorithm, we generated cw and ccw (circular) trajectories. We show sample cw (C) and ccw (D) trajectories. The center for the circle i (or i^{th} trajectory), (x_i^c, y_i^c), is sampled from a uniform distribution $(1500 < x_i^c \& y_i^c < 5000)$ and its radius (R_i) is sampled from a normal distribution $(R_i \sim N(\mu_R, \sigma_R)$ with $\mu_R = 1000$ and $\sigma_R = 50$, shown with vertical dotted lines on the histograms. $x_{ji} = x_i^c + R_i \cos(\theta_j)$ and $y_{ji} = y_i^c + R_i \sin(\theta_j)$ are the coordinates of the j^{th} point on the i^{th} circle. θ_j goes from 0 to 2π for a ccw circle, while it goes from 2π to 0 for a cw circle, both with uniform steps of $2\pi/360$. We use our algorithm to calculate μ_R and σ_R from the generated data. We show histograms of inverse average curvatures for 500 circular cw (E) and ccw (F) trajectories. The dashed vertical lines show the theoretical values of μ_R. We show histograms of the standard deviation of the inverse average curvature for cw (G) and ccw (H) trajectories. The dashed vertical lines show the theoretical values of σ_R.

II. Density calculation

Density profiles shown in Figs. 3 and 4, and Figs. S4 and S7 are calculated as follows: concentric circular rings – of radius r_i – are considered around the center of the beads. The density at r_i is calculated according to $n_i = N_i/dA_i$, where N_i is the number of frames (points) within the area between r_i and r_{i+1}, and $dA_i = A_{i+1} - A_i$ where A_i is πr_i^2. Background densities are calculated with respect to points

away from the bead center. Density enhancements are calculated as the density with respect to the bead center divided by the average background density at various distances from the bead center. All densities are taken from motile bacteria only.

III. Modeling hydrodynamic interactions of BV with surfaces and spherical objects

To simulate BV's behavior between two opposing surfaces, we adapted a model presented in Ref. 1. We considered the surfaces far enough apart that the effect of one surface doesn't effect the other surface. In addition, we implemented a model from Ref. 2 to simulate BV's interaction with spherical beads.

We briefly summarize key parts of both models here – with equations superscripted s for BV's interaction with surfaces, and equations superscripted b for BV's interaction with beads – from Refs. 1, 2. The readers are referred to Refs. 1, 2 for additional details.

A far field hydrodynamic model is used in both cases. We modeled BV as a prolate spheroid, with a flagellum, in order to be able to use Faxén's laws (1). BV's dynamics can be modeled near a flat, no-slip surface using a linear combination of four hydrodynamic terms with Brownian fluctuations; to clarify, a no slip surface implies that the fluid velocity near the boundary approaches zero. The first of these terms, a force dipole, arises from the opposing directions of the flow field around the moving object. Higher order approximations lead to the other three terms: a force quadrupole term (due to the nonuniform flow fields around the body length), a source dipole (due to difference in hydrodynamic potential across the body), and a rotlet dipole (due to the opposing rotation of the body and the flagellum).

The rotlet dipole creates a rotation along an axis perpendicular to the surface (a qualitative effect observed in many bacteria near surfaces). The model also describes the orbiting of BV around beads. For this effect, only the force dipole term was considered, since BV must get much closer to a curved object for higher order terms to be necessary.

The actual terms are described using derivatives of a Green's function for the linearized Navier-Stokes equations (a stokeslet). This approximation is known to be valid for low Reynold's numbers.

We define two different coordinate systems: $\vec{r}_s$, $\vec{r}_s^{\perp}$ and $\vec{r}_b$,$\vec{r}_b^{\perp}$. Both $\vec{r}_s$ and $\vec{r}_b$ represent the components of the orientation vector $\vec{e}$ (BV's director) in the direction of the normal line connecting the surface and the BV and the normal line connecting the bead and the BV, respectively. To complete the decompositions, we consider the directions $\vec{r}_s^{\perp}$ and $\vec{r}_b^{\perp}$ as the remaining component of the orientation vector for each model, respectively (1, 2)

$$\vec{r_b} = \frac{\vec{x} - \vec{x}_b}{\|\vec{x} - \vec{x}_b\|} \tag{9}$$

$$\vec{r_b^{\perp}} = \frac{\vec{e} - (\vec{e} \cdot \vec{r}_b)\vec{r}_b}{\|\vec{e} - (\vec{e} \cdot \vec{r}_b)\vec{r}_b\|} \tag{10}$$

where $\vec{x}_b$ is the center of the spherical object. The terms for calculations near a surface were defined similarly.

The magnitude of the hydrodynamic forces on BV are proportional to the distance between BV's center of mass and the surface (or bead). We therefore define these distances as h_s and h_b respectively. The magnitude of the forces is related to BV's orientation angle with respect to each object. We therefore define the angle θ_s as

$$\theta_s = cos^{-1}\Big(\frac{\vec{v} \cdot \vec{r_s^{\perp}}}{\|\vec{v}\|\|\vec{r_s^{\perp}}\|}\Big). \tag{11}$$

θ_b is defined in the same way as above (2). If $(\vec{x} - \vec{x}_b) \cdot \vec{v} < 0$ we used $-\theta$ instead since the inverse cosine does not give a direction of the angle. $\vec{v}$ is BV's normalized natural velocity and is, therefore, equivalent to the orientation vector.

The dynamical equations for BV are then defined as:

$$d\vec{x}(t) = (\vec{v} + \vec{u})dt + \sqrt{6D}d\vec{B}_1(t) \tag{12}$$

$$d\vec{e}(t) = (\vec{\Omega}dt + \sqrt{4D_r}d\vec{B}_2(t)) \times \vec{e} \tag{13}$$

where $\vec{\Omega}$ is the hydrodynamic contribution to the torque, $\vec{u}$ is the hydrodynamic contribution to the velocity, and D and D_r are the translational and rotational diffusion constants, respectively. $\vec{B}_1(t)$ is a normal Brownian motion, while $\vec{B}_2(t)$ is a Brownian motion on a sphere. We assume that the bacterium does not directly contribute to the torque (which is observed in experiments).

The model is scaled according to the length of the body of the bacterium and the (assumed constant mean) velocity of the bacterium in free space. Time (t) is non-dimensionalized with respect to these two parameters (bacterium body length and its velocity). We assumed that the BV cannot be less than 1 of its radii away from a surface or bead (hard wall repulsion). The hydrodynamic contributions are, as

previously stated, a linear combination of terms such that:

$$\vec{u}^s = \vec{u}^s_{FD} + \vec{u}^s_{FQ} + \vec{u}^s_{SD} + \vec{u}^s_{RD} \tag{14}$$

$$\vec{u}^b = \vec{u}^b_{FD} \tag{15}$$

$$\vec{\Omega}^s = \vec{\Omega}^s_{FD} + \vec{\Omega}^s_{FQ} + \vec{\Omega}^s_{SD} + \vec{\Omega}^s_{RD} \tag{16}$$

$$\vec{\Omega}^b = \vec{\Omega}^b_{FD} \tag{17}$$

$$\vec{u}^s_{FD} = \frac{-3\alpha(1-3sin^2(\theta_s))}{8h_s^2}\vec{r}_s + \frac{3\alpha sin(2\theta_s)}{8h_s^2}\vec{r}^{\perp}_s; \text{(Eq. B6 in Ref. 1)} \tag{18}$$

$$\vec{u}^s_{FQ} = \frac{\beta sin(\theta_s)}{4h_s^3}(7-9sin^2(\theta_s))\vec{r}_s + \frac{\beta cos(\theta_s)}{16h_s^3}(7-27sin^2(\theta_s))\vec{r}^{\perp}_s; \text{(Eq. B9 in Ref. 1)} \tag{19}$$

$$\vec{u}^s_{SD} = \frac{-\zeta sin(\theta_s)}{h_s^3}\vec{r}_s + \frac{-\zeta cos(\theta_s)}{4h_s^3}\vec{r}^{\perp}_s; \text{(Eq. B14 in Ref. 1)} \tag{20}$$

$$\vec{u}^s_{RD} = 0; \text{(Eq. B17 in Ref. 1)} \tag{21}$$

$$\vec{u}^b_{FD} = \frac{-3A\delta(1-3sin^2(\theta_b))(A+h_b)}{2h_b^2(2A+h_b)^2}\vec{r}_b + \frac{3A^3\delta(2A^2+6Ah_b+3h_b^2)sin(2\theta_b)}{4h_b^2(A+h_b)^3(2A+h_b)^2}\vec{r}^{\perp}_b; \text{(Eq. 39 in Ref. 2)} \tag{22}$$

$$\vec{\Omega}^s_{FD} = \frac{-3\alpha sin(2\theta_s)}{16h_s^3}(1+\frac{\Gamma}{2}(1+sin^2(\theta_s))\vec{r}^{\perp}_s \times \vec{r}_s; \text{(Eq. B6 in Ref. 1)} \tag{23}$$

$$\vec{\Omega}^s_{FQ} = \frac{-3\beta cos(\theta_s)}{8h_s^4}(1-3sin^2(\theta_s)+\frac{\Gamma}{4}(11-3sin^4(\theta_s)))\vec{r}^{\perp}_s \times \vec{r}_s; \text{(Eq. B10 in Ref. 1)} \tag{24}$$

$$\vec{\Omega}^s_{SD} = \frac{3\zeta cos(\theta_s)}{8h_s^4}(1+\frac{3\Gamma}{2}(1+sin^2(\theta_s))\vec{r}^{\perp}_s \times \vec{r}_s; \text{(Eq. B14 in Ref. 1)} \tag{25}$$

$$\vec{\Omega}^s_{RD} = \frac{\nu cos(\theta_s)}{16h_s^3}(5-3\Gamma sin^2(\theta_s))\vec{r}_s + \frac{\nu sin(\theta_s)}{16h_s^3}(2+3\Gamma cos^2(\theta_s))\vec{r}^{\perp}_s; \text{(Eq. B17 in Ref. 1)} \tag{26}$$

$$\vec{\Omega}^b_{FD} = \frac{-3\delta A^3 sin(2\theta_b)}{4h_b^3(A+h_b)^2(2A+h_b)^3}\Big(2A^2+6Ah_b+3h_b^2-\frac{\Gamma Q}{8A^2(A+h_b)^2}\Big)\vec{r}^{\perp}_b \times \vec{r}_b; \text{(Eq. 40 in Ref. 2)} \tag{27}$$

$$Q = A^6 - 5A^4(A+h_b)^2 + 10A^2(A+h_b)^4 + 6(A+h_b)^6 + (9A^6 - 29A^4(A+h_b)^2 + 34A^2(A+h_b)^4 - 18(A+h_b)^6)cos(2\theta_b); \text{(Eq. 41 in Ref. 2)} \tag{28}$$

$$\Gamma = \frac{1-\gamma^2}{1+\gamma^2} \tag{29}$$

where γ is the aspect ratio (defined as the width divided by the length) of the bacterial body, α,β,ζ,ν, and δ (as dimensionless model parameters) are the strengths of the multipoles. FD, FQ, SD, and RD stand for force dipole, force quadrupole, source dipole, and rotlet dipole respectively. A is the radius of the spherical object. These terms are derived using the method of images (1, 2). The fluid flows under

the given boundary conditions can be constructed by placing identical swimmers behind the boundary. The image swimmers allow one to construct the unique flow field such that the boundary conditions are satisfied. These equations were simulated using a forward Euler algorithm. To prevent BV from moving through a wall, the component of BV's velocity in the direction of the wall was set to zero if a time step would move it beyond the wall.

Using a hydrodynamic model for BV's interaction with opposing surfaces, we have shown that our simulations are consistent with the experimental observation that bacteria rotate clockwise near the top of a coverslip (viewed from below; view direction being +z direction). The simulations show that BV switches its direction of rotation as it moves to the opposing surface, consistent with experimental observations. The radius of the circles depends on the distance to the surface, the strength of the rotlet dipole (which depends on the shape and propulsion mechanism of each individual bacterium), and the aspect ratio of the bacterium (Eq. 3.8 in Ref. 1). However, this is the relationship for a single surface. In our model, we looked at the motility of BV between two opposing surfaces, and thus the rotlet dipole is the sum of the rotlet dipoles from the top and bottom surface. In particular, assuming that the bacterium is parallel to the surfaces, we have a generalization of Eqs. 3.7 and 3.8 in Ref. 1 as follows:

$$z \cdot \Omega = -\frac{3\nu}{32h^4}(1-\Gamma) + \frac{3\nu}{32(h_{top}-h)^4}(1-\Gamma) \tag{30}$$

Therefore:

$$R_\tau = \frac{32}{3|\nu|(1-\Gamma)} \frac{(h(h_{top}-h))^4}{h^4-(h_{top}-h)^4}. \tag{31}$$

Clearly we see that this radius is infinite midway between the two planes (one surface being set to 0, and the other to h_{top}) no matter the parameters. This will always be where the direction of rotation changes and is consistent with our experimental and theoretical results. In addition, distance was nondimensionalized by the length of the semi-major axis of the bacterium.

Therefore, since *E.coli* has a much larger length than BV, it will generally swim in circles having a much larger radius. Furthermore, BV and *E. coli* have different rotlet dipole strengths as well as different aspect ratios. Although the effects of the last two factors are difficult to determine, it is expected that hydrodynamic effects would be stronger in BV than *E. coli* since BV generates larger hydrodynamic flows with respect to its body size and mass than *E. coli* resulting in the differences stated above.

In our model, the forces are scaled by the body length, free swimming velocity and viscosity. Therefore

in Eq. 30 we see that the radius will depend on viscosity, assuming that the dimensional angular velocity is fixed. For our experiments, this is expected to be the case. Therefore, we expect the swimming radius of our BV to increase with viscosity as observed in Fig. S4.

Furthermore, using a hydrodynamic model for BV's interaction with spherical beads, we show BV's capture probability vs bead radius increases. For a bead of $A = 2$ (roughly the size of *E. coli*), our model predicts there is no capture for BV. Our simulations show that *E. coli* is too small to capture a BV. The results of these simulations are shown in Fig. S2.

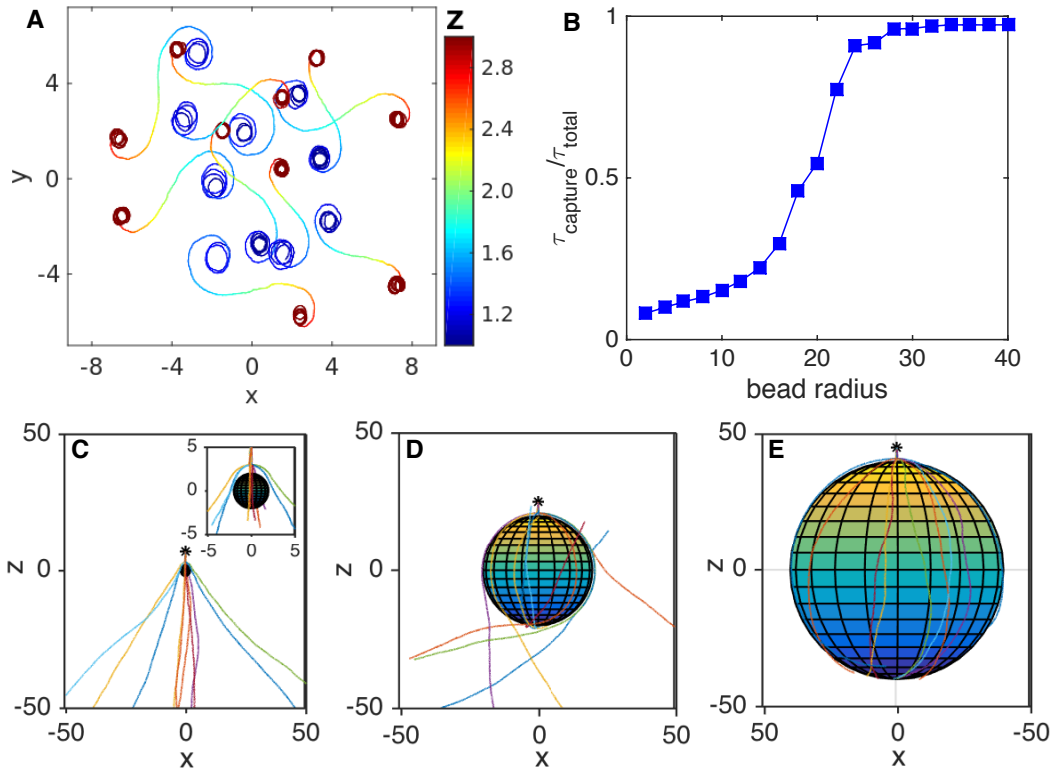

FIGURE S2. Our hydrodynamic model (given in Supplementary Text) predicts strong hydrodynamic interactions of BV with surfaces and spherical obstacles. (A) Here we show sample simulated trajectories of BV between two opposing surfaces. The color bar represents z. BV rotate in circular trajectories on the surfaces and show a rotational direction switch when moving from one surface to the other, with an increase in the curvature radius as it moves away from surfaces. The surfaces are set, arbitrarily, at $z = 0$ and $z = 4$. As for parameters (all dimensionless and defined in Supplementary Text), $D = 0.03$, $D_r = 0.75 \times D$, $\alpha = 0.8$, $\beta = -0.01$, $\zeta = 0.1$, $\nu = 12$, and $\gamma = 0.3$. All trajectories start with the same initial velocity, but with uniform random initial positions at $z = 1.01$ (within the shown xy range), and run from $t = 0$ to 30. To re-emphasize, equations with superscript s (given in Supplementary Text) are used for the part of simulation shown in this subplot. (B) BV's capture probability vs bead radius is shown as predicted by our hydrodynamic model for BV's interaction with spherical beads. Our metric compared the time the BV was circling the bead ($\tau_{capture}$) with the total simulation time (τ_{total}). As can be seen, BV is easily captured for larger beads, and the probability of capture goes to zero for beads the size of prey. In (C to E), reproduced for convenience, we show 10 sample trajectories of BV for $\delta = 0.8$ (the force dipole strength near the beads) around three instances of beads with radii of $A = 2$, 20, and 40, respectively, in units of the bacterial body length. All trajectories started at $(A+5, 0, 0)$, initially in -z direction, and ran from $t = 0$ to 120. The dimensionless diffusion coefficient is $D = 2.5 \times 10^{(-2)}$ here. To reemphasize, equations with superscript b (given in Supplementary Text) are used for the part of the simulation shown in (B to E). The probability of capture goes from 0 to 1 from (C) to (E). This capture probability is an upper bound. In real experiments, bacteria lose their orbit around beads by interacting with the neighboring surface on which the bead rests. The model excludes the possibility of interaction of bacteria with surfaces neighboring beads while on the bead (which reduces the bacterium's capture time). In addition, the model also excludes the possibility of collision of captured bacteria with debris, dead bacteria, and surface imperfections of the bead.

We have found no simple analytical expression relating the radius of the trajectories on the surface and the capture radius of a bead. In general, we can only say that the distance of the bacterium to the surface, the strength of the rotlet dipole and the aspect ratio of the bacterium contribute to the radius of the circular trajectory on the plane, while the bacterium's aspect ratio as well as the force dipole strength (Eq. 15 in Ref. 2) primarily contributes to the radius of the sphere above which there is effective capture.

BV's flagellar motor rotary state.

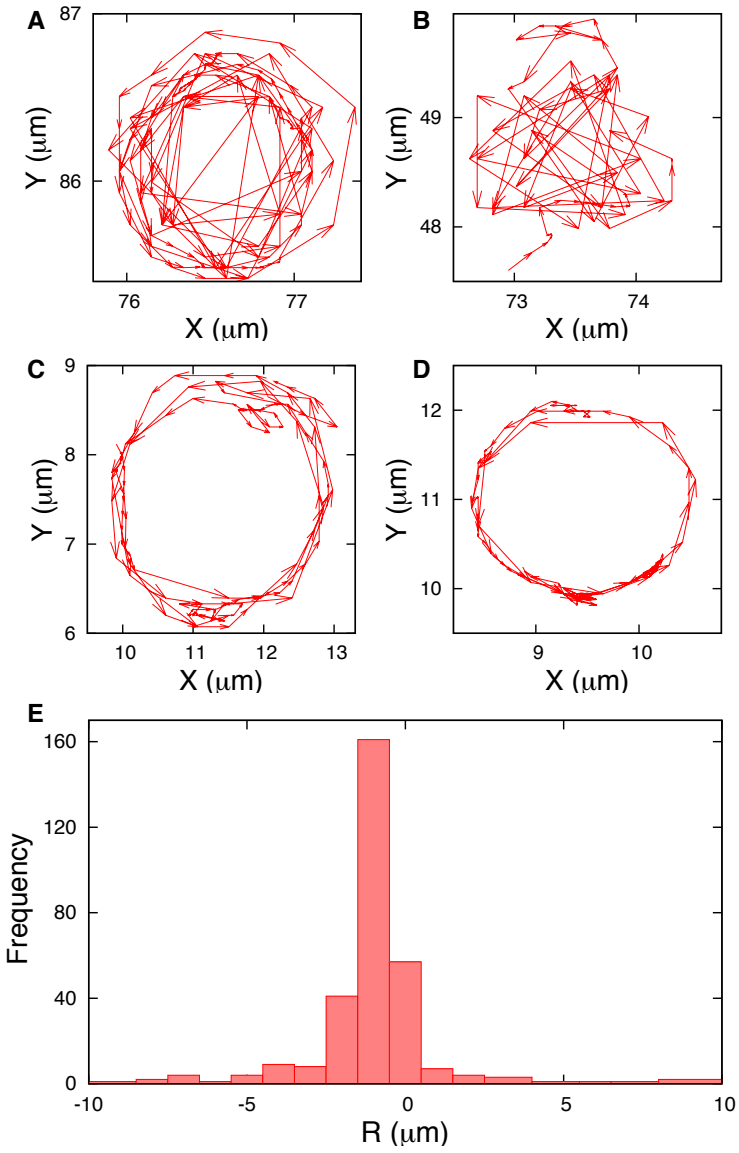

FIGURE S3. BV's flagellar motor rotates primarily in one direction (counterclockwise, ccw). BV's flagellum was tethered to coverslips (3) and their bodies' rotation recorded and analyzed (4). Here we show trajectories for four instances of BV's body rotation around the attachment point (at its flagellum) (A to D). A histogram for the effective radius (Supplementary Text) is given in (E). This analysis shows a strong bias in the rotation direction of the flagellum; the flagellum rotates effectively ccw when seen from its tip. Negative effective radius values (E) coincide with ccw rotations, while positive values coincide with clockwise (cw) rotations. Exclusively for this part of the experiments, we used BV strain 109J because its body is rather longer than strain 109, and this feature makes it possible to easily monitor its body's rotation.

Change in BV's trajectory curvature vs viscosity of the solution.

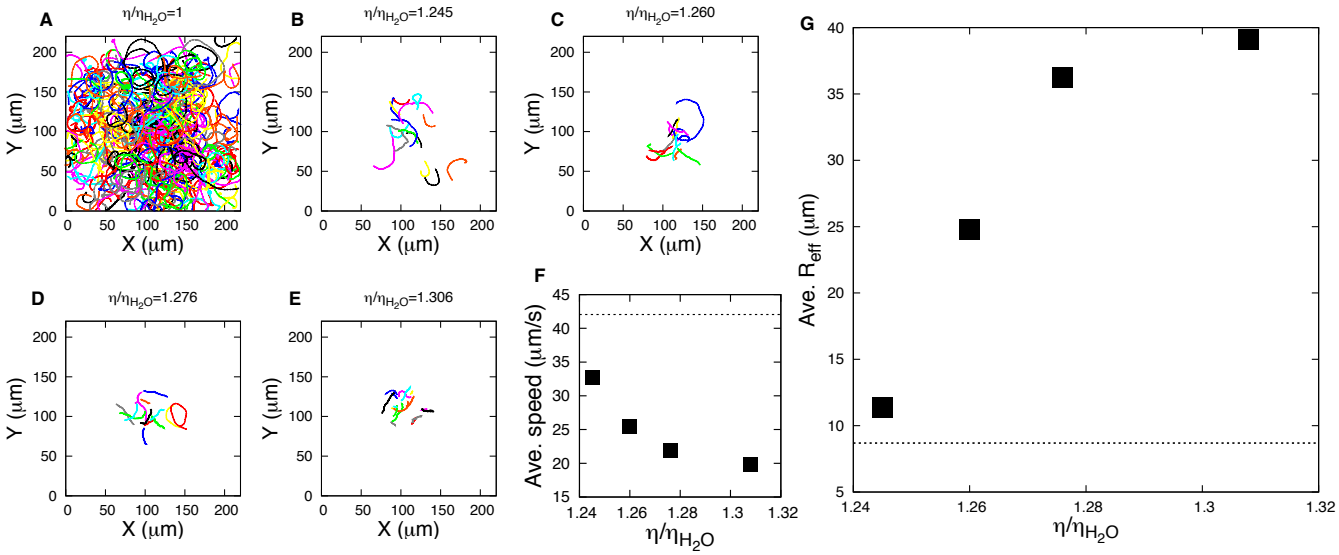

FIGURE S4. BV's trajectories straighten as the viscosity of the solution increases. Viscous solutions were prepared according to Tables 130 and 131 in Ref. 5, and BV trajectories were recorded on the coverslip. Here we show BV trajectories (A to E) from control ($\eta/\eta_{H_2O} = 1$) to highest viscosity. We show both BV's swimming speed (mean out of about 15 trajectories) vs viscosity (F), and the average effective radius of the trajectories vs viscosity (G). The dotted lines represent the corresponding values for the control ($\eta/\eta_{H_2O} = 1$).

BV and *E. coli* motility along walls.

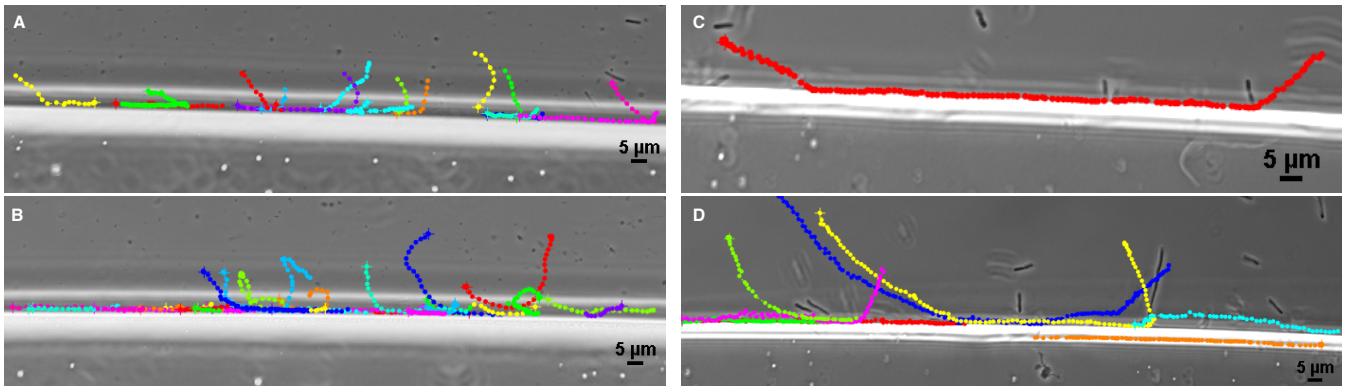

FIGURE S5. BV and *E. coli* move in straight trajectories along the walls. The wall is constructed according to the recipe provided in Materials and Methods. Healthy BV or *E. coli* solutions were then introduced against the edge of the wall. Sample BV (A and B) and *E. coli* (C and D) trajectories are shown with the bacteria swimming in (almost) straight lines along the edges of hard walls. Their behavior near walls motivated our study of the behavior near beads.

BV motility around electrically inert beads with varying radii.

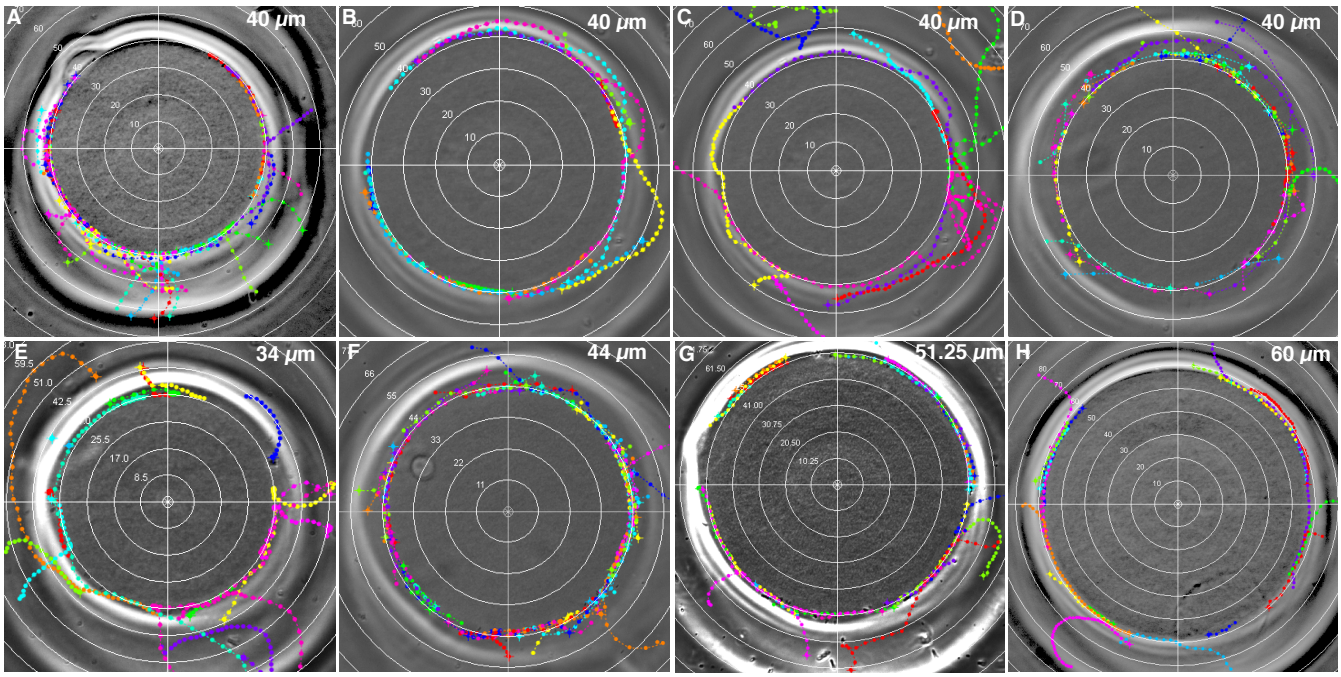

FIGURE S6. BV orbit around inert and electrically neutral beads of various radii. Here we show sample trajectories of BV around inert CL beads with radii ranging from $34 - 60\mu m$ (the density analysis we discuss in the next figure sets error bars of about $1 - 2\mu m$ on these sizes). We show sample trajectories demonstrating BV orbit around different beads with the same radii ($40\mu m$) (A to D), and for beads with varying radii ($34 - 60\mu m$) (E to H). The grid steps are as follows: (A to D) $10.00\mu m$, (E) $8.50\mu m$, (F) $11.00\mu m$, (G) $10.25\mu m$, and (H) $10.00\mu m$.

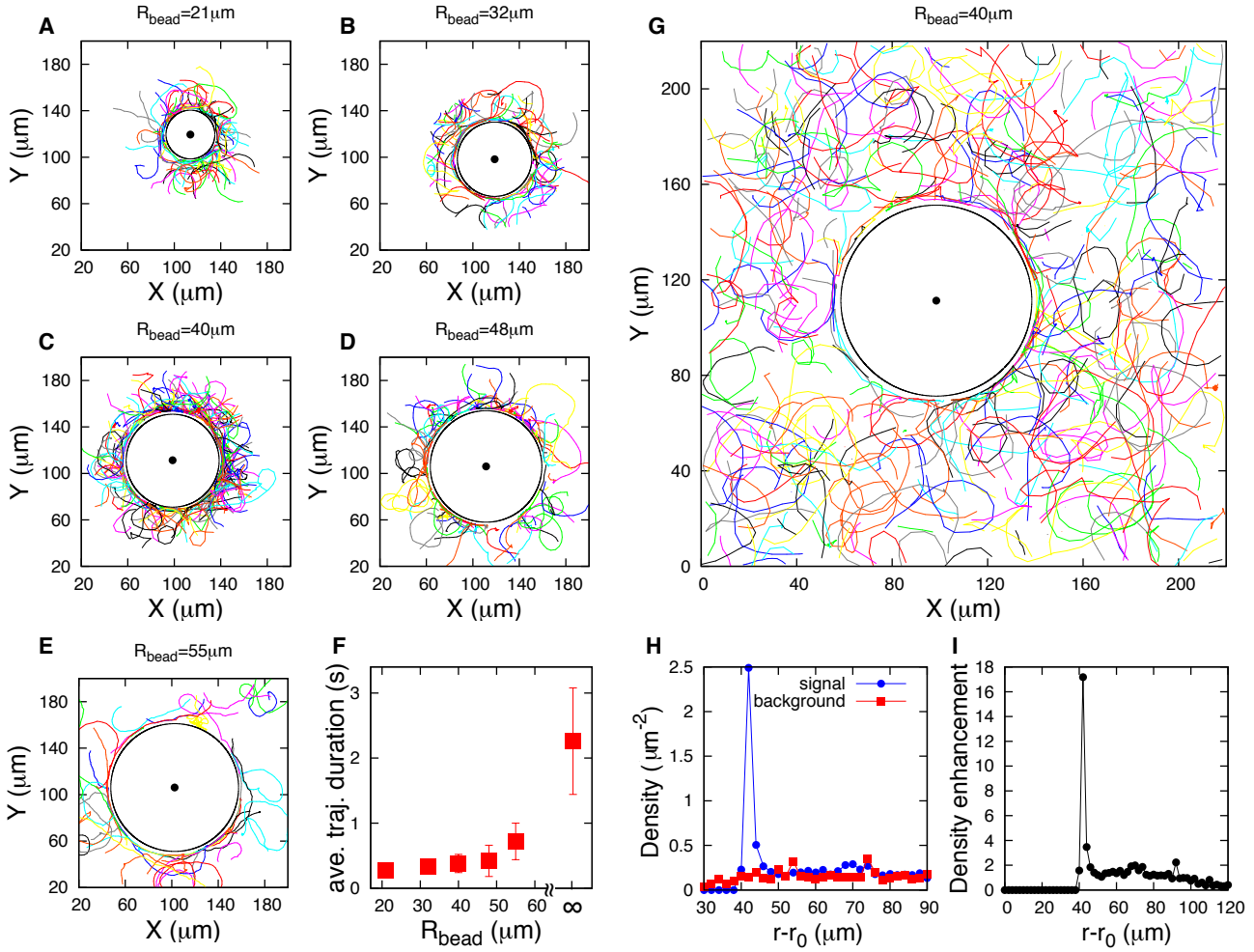

FIGURE S7. BV orbit and localize around inert and electrically neutral beads of various radii. The capture time around beads increases along with the bead radius. Here we show sample trajectories demonstrating BV orbiting and localizing around inert CL beads with radii ranging from $21 - 55\mu m$ (A to E). Total number of trajectories analyzed in (A to E) are 80, 119, 149, 80, and 51, respectively, and they are tracked within an area of $20\mu m$ from the bead surface (the central dot shows bead center). Mean capture time – defined as the average duration of the trajectories within $5\mu m$ from each bead surface – increases with the bead radius (F) where the data point at $R_{bead} = \infty$ shows average trajectory durations on the surface of the coverslip and slide (from Fig. **??**, B and D), as an upper limit of an infinite radius bead. For each data point, 5% of outliers are dropped from each side since long dwells indicate bacteria are stuck to surfaces while short dwells are associated with trajectories grazing, but never being captured, by beads. In (G) we show 333 BV trajectories tracked everywhere around the bead with their density profile in (H). Red line with squares in (H) represents the background density, which is the sum of densities calculated with respect to the four corner points in (G), while the blue line with filled circles is density with respect to bead center. In (I) we show the density enhancement which is the density with respect to the bead center (blue in H) divided by the average background density (red in H).

BV motility around electrically charged beads.

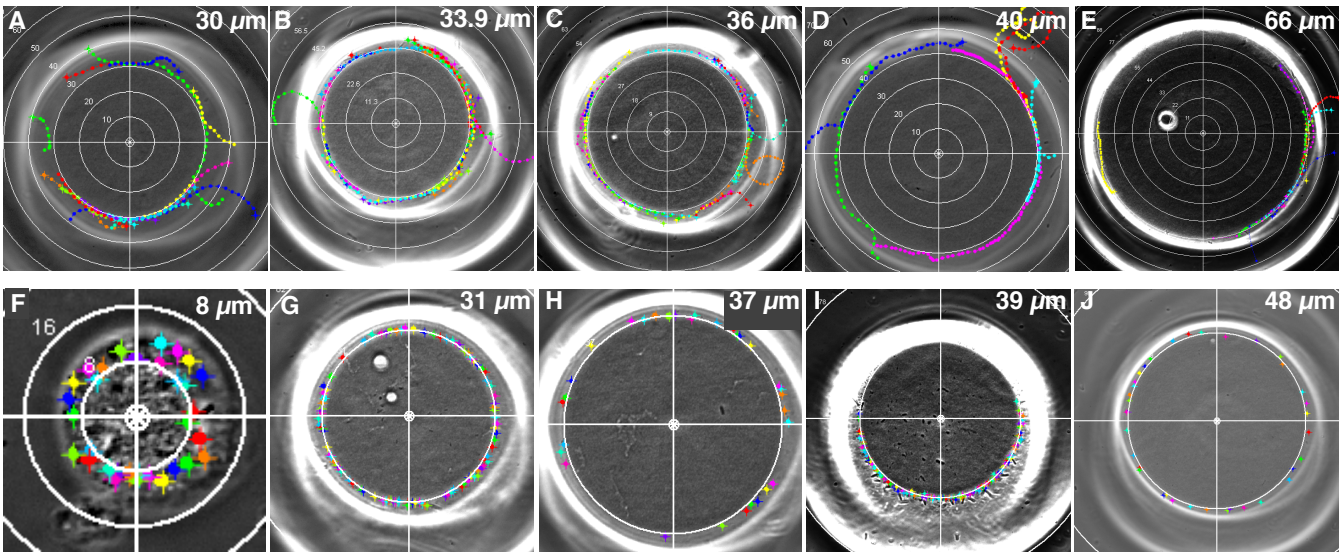

FIGURE S8. BV localize and orbit around slightly negatively-charged SP beads, while they accumulate and lose motility around positively-charged DEAE beads. Since bacteria have electrically charged membranes, geometric capture could be due to favorable electrostatic interaction between BV and the bead. For this reason, we studied the interaction of the predator as well as prey with electrically charged beads. We used electrically positive DEAE beads and electrically negative SP beads – see Materials and Methods – with different radii and we studied BV's and *E. coli*'s motility around them. The results are shown here for BV, and in the next figure (Fig. S9) for *E. coli*. The behavior of the predator is similar to that of the prey around each bead. Both circle around negatively-charged beads, although the capture strength is weaker compared to inert beads because the electrical repulsion cancels out a portion of the hydrodynamic attractive force. On the other hand, they both accumulate and stick around positively-charged beads. In this case, both the electrostatic attraction and hydrodynamic forces attract BV to the surface of the bead. Thus, numerous bacteria stick to the bead surface and lose mobility immediately after mixing beads and bacteria. Typical BV trajectories are shown around negatively-charged SL beads in (A to E), for beads with radii ranging from $30-66\mu m$. In (F to J) we show BV electrostatically trapped on positive DEAE beads with radii as small as $8.00\mu m$ up to approximately $50.00\mu m$. The radius for each bead is given on each figure. The grid steps are as follows: (A) $10.00\mu m$, (B) $11.30\mu m$, (C) $9.00\mu m$, (D) $10.00\mu m$, (E) $11.00\mu m$, (F) $8.00\mu m$, (G) $31.00\mu m$, (H) $37.00\mu m$, (I) $39.00\mu m$, and (J) $48.00\mu m$.

E. coli motility around electrically charged beads.

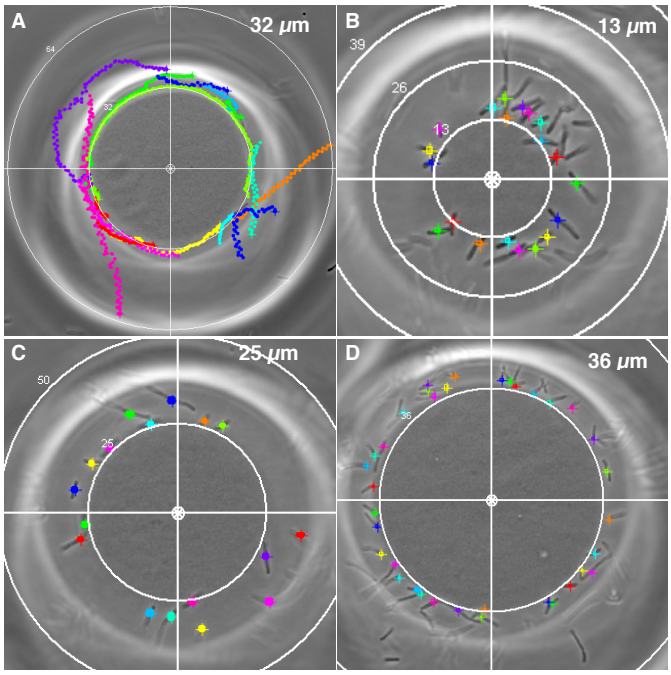

FIGURE S9. *E. coli* localize and orbit around negatively-charged SP beads, while they become electrostatically trapped and lose motility around positively-charged DEAE beads. We show sample *E. coli* trajectories around a negatively-charged bead of approximate radius $32\mu m$ (A). In (B to D), we show trapped *E. coli* cells on the surfaces of the positively-charged beads with radii $13.00\mu m$ to $36.00\mu m$. The radius for each bead is given on each figure. The grid steps are as follows: (A) $32.00\mu m$, (B) $13.00\mu m$, (C) $25.00\mu m$, (D) $36.00\mu m$.

Supporting Movies

Movie S1. BV on coverslip

In this video we show BV's motility on the coverslip surface. Solution containing BV is sandwiched between a coverslip and a microscope slide. The view is from the coverslip. The same video is shown in two panels; left panel without tracks, right panel with tracks.

Movie S2. BV in midplane

In this video we show BV's motility in the midplane between coverslip and slide. Solution containing BV is sandwiched between a coverslip and a microscope slide. The view is from the coverslip. The same video is shown in two panels; left panel without tracks, right panel with tracks.

Movie S3. BV on slide

In this video we show BV's motility on the slide surface. Solution containing BV is sandwiched between a coverslip and a microscope slide. The view is from the coverslip. The same video is shown in two panels; left panel without tracks, right panel with tracks.

Movie S4. BV on CL bead

In this video we show BV orbiting around an inert and electrically neutral CL bead (resting on the coverslip). Solution containing BV (mixed with beads) is sandwiched between the coverslip and the microscope slide. The view is from the coverslip.

Movie S5. *E. coli* on CL bead

In this video we show *E. coli* orbiting around an inert and electrically neutral CL bead (resting on the coverslip). Solution containing *E. coli* (mixed with beads) is sandwiched between the coverslip and the microscope slide. The view is from the coverslip.

References

1. Spagnolie, S. E., and E. Lauga. 2012. *Hydrodynamics of self-propulsion near a boundary: predictions and accuracy of far-field approximations. J. Fluid Mech.* 700:105-147.

2. Spagnolie, S. E., G. R. Moreno-Flores, D. Bartolo, E. Lauga. 2015. Geometric capture and escape of a microswimmer colliding with an obstacle. *Soft Matter.* 11:3396-3411.

3. Gabel, C. V., and H. C. Berg. 2003. The speed of the flagellar rotary motor of *Escherichia coli* varies linearly with protonmotive force. *Proc. Nat. Acad. Sci. USA* 100:8748-8751.

4. Qian, C., C. C. Wong, S. Swarup, and K.- H. Chiam. 2013. Bacterial tethering analysis reveals a run-reverse-turn mechanism for *Pseudomonas* species motility. *Am. Soc. Microbiol.* 79:4734-4743.

5. Swindells, J. F., C. F. Snyder, R. C. Hardy, and P. E. Golden. 1958. Viscosities of sucrose solutions at various temperatures: Tables of recalculated values. *Supplement to National Bureau of Standards Circular.* 440:1-7.